Arabian Journal of Chemistry (2016) xxx, xxx–xxx

King Saud University

Arabian Journal of Chemistry

www.ksu.edu.sa
www.sciencedirect.com

ORIGINAL ARTICLE

Synthesis and photoelectrical characterizations of ECPPQT for optoelectronic application

A.A.M. Farag [a,b,*], Magdy A. Ibrahim [c], Nasser M. El-Gohary [c], N. Roushdy [d]

[a] *Thin Film Laboratory, Department of Physics, Faculty of Education, Ain Shams University, Roxy, 11711 Cairo, Egypt*
[b] *Department of Physics, Faculty of Science and Arts, Aljouf University, Saudi Arabia*
[c] *Department of Chemistry, Faculty of Education, Ain Shams University, Roxy, 11711 Cairo, Egypt*
[d] *Electronic Materials Department, Advanced Technology and New Material Institute, City for Scientific Research and Technological Applications, New Borg El Arab City 21934, Alexandria, Egypt*

Received 10 October 2015; accepted 1 January 2016

KEYWORDS

Heteroannulated chromones;
^{1}H NMR;
IR;
Mass spectra;
Optical properties;
Optoelectronic

Abstract A new derivative of heteroannulated chromeno[2,3-*b*]pyridine identified as 5-ethyl-7*H*,9*H*-chromeno[3″,2″:5′,6′]pyrido[3′,2′:5,6]pyrano[3,2-*c*]quinoline-6(5*H*),7,9-trione (**3**) (**ECPPQT**) was easily and efficiently synthesized from DBU catalyzed condensation reaction of 2-aminochromone-3-carboxaldehyde (**1**) with 6-ethyl-4-hydroxy-2*H*-pyrano[3,2-*c*]quinoline-2,5(6*H*)-dione (**2**). Structure of **ECPPQT** was deduced based on its correct elemental analysis and spectral data (IR, ^{1}H NMR, and mass spectra). The X-ray diffraction patterns of TCVA in powder form show that there are several peaks with different intensities, indicating that the material has a polycrystalline nature. Optical absorption properties of **ECPPQT** thin films in near ultraviolet, visible and near infrared spectral regions showed characteristic absorption peaks. Optical absorptions were used to determine the characteristic band transitions in the range of 200–1100 nm. Two direct band gaps were calculated and found to be 1.85 and 3.30 eV for the optical and transport energy gaps, respectively. The **ECPPQT**/p-Si diode performs low photovoltaic characteristics with open circuit voltage of 330 mV, short-circuit current of 37 μA and fill factor of 33%. The phototransient measurements of the device indicate that the device has a good stability and quick response properties.

1. Introduction

Chromones are well-known natural and synthetic products that possess diverse biological activities (Keri et al., 2014), including anticancer (Valenti et al., 2000; Lim et al., 2000; Shi et al., 2001), antitumor (Huang et al., 2009), antiproliferative (Huang et al., 2013), neuroprotective (Larget et al., 2000), HIV-inhibitory (Ungwitayatorn et al., 2004; Ishakava et al., 1999), antimicrobial (Göker et al., 2005; Deng et al., 2000), antioxidant (Pietta, 2000), anti-inflammatory (Mazzei et al., 1999) and antibiotic (Albrecht et al., 2005). Heteroannulated chromones showed significant biological activity including

* Corresponding author at: Thin Film Laboratory, Department of Physics, Faculty of Education, Ain Shams University, Roxy, 11711 Cairo, Egypt. Tel.: +20 26979854; fax: +20 22581243.
E-mail addresses: alaafaragg@edu.asu.edu.eg, alaafaragg@gmail.com (A.A.M. Farag).
Peer review under responsibility of King Saud University.

ELSEVIER Production and hosting by Elsevier

http://dx.doi.org/10.1016/j.arabjc.2016.01.002
1878-5352 © 2016 Production and hosting by Elsevier B.V. on behalf of King Saud University.
This is an open access article under the CC BY-NC-ND license (http://creativecommons.org/licenses/by-nc-nd/4.0/).

Please cite this article in press as: Farag, A.A.M. et al., Synthesis and photoelectrical characterizations of ECPPQT for optoelectronic application. Arabian Journal of Chemistry (2016), http://dx.doi.org/10.1016/j.arabjc.2016.01.002

pharmacological (Singh et al., 2002), antiplatelet (Chang et al., 2002), antiallergic (Nohara et al., 1985), antiangiogenic (Lee et al., 2005), antirheumatic (Ukawa et al., 1985), antibacterial (Podos et al., 2012), anti-inflammatory and analgesic (Hosni and Abdulla, 2008). Friedländer condensation of 2-aminochromone-3-carboxaldehyde is a well-known reaction for preparation of chromeno[2,3-*b*]pyridine derivatives (Siddiqui et al., 2010; Ibrahim, 2010; Ibrahim et al., 2009; Siddiqui, 2012). The present work aimed to study the chemical reactivity of 2-aminochromone-3-carboxaldehyde (**1**) with 6-ethyl-4-hydroxy-2*H*-pyrano[3,2-*c*]quinoline-2,5(6*H*)-dione (**2**) as a heterocyclic enol under basic conditions, using 1,8-diazabicyclo[5.4.0]undec-7-ene (DBU) as a basic catalyst, hoping to construct a novel derivative of heteroannulated chromeno[2,3-*b*]pyridines.

It is well known that organic based electronic devices attract considerable attention due to their particular multiple advantages such as easy and cheap processing, low cost of fabrication, possibility of chemical modifications, and low temperature processing and have a compatibility with inorganic semiconductors (Li et al., 2015; Zhou et al., 2012; Carroll et al., 2011; Knipp, 2006). These unique competitive characteristics make them highly compatible for organic solar cells, nonlinear electrical conductors, organic memory devices, organic thin film transistors, photographic technology, organic light emitting diodes, organic photodetectors and organic sensors (Elkington et al., 2014; Newman et al., 2004; Liu et al., 2011; Peumans et al., 2003; James et al., 2005; Yakuphanoglu and Arslan, 2007). Knipp (2006) has confirmed that the quality of organic electronic devices is strongly dependent on the type of preparation technique as well as the controlling processing parameters. These characteristics have supported much research for the preparation of organic thin films with particular simple and low cost techniques which offer large area deposition with low temperature synthesis such as spray process (Ashour and El Sayed, 2009), dip-coating (Cremonesi et al., 2006), chemical bath deposition (Chavhan et al., 2008), successive ionic layer adsorption and reaction (SILAR) (Laukaitish et al., 2000) and spin coating (Sahu et al., 2009). Spin coating is one of the most appropriate techniques to prepare **ECPPQT** thin films with low cost, controlled parameters, highly adherence and nearly homogeneous characteristics.

The objective of this work was devoted to synthesis a new derivative of heteroannulated chromeno[2,3-*b*]pyridine, identified as 5-ethyl-7*H*, 9*H*-chromeno[3″,2″:5′,6′]pyrido[3′,2′:5,6]pyrano[3,2-*c*]quinoline-6(5*H*), 7,9-trione (**3**) (**ECPPQT**). Moreover, morphological and crystalline structure of thin films was checked by X-ray diffraction (XRD) and scanning electron microscopy (SEM). Optical absorption and energy gap of the films as well as photoluminescence characteristics were also considered. Additional support to the work was achieved by the results of diode based **ECPPQT** for optoelectronic application.

2. Experimental details

2.1. Reactions and molecular structure characterization

A mixture of 2-aminochromone-3-carboxaldehyde (**1**) (0.57 g, 3 mmol) and 6-ethyl-4-hydroxy-2*H*-pyrano[3,2-*c*]quinoline-2,5(6*H*)-dione (**2**) (0.77 g, 3 mmol), in DMF (15 mL) containing DBU (0.1 mL) was heated under reflux for 2 h. The yellow crystals obtained during heating were filtered and crystallized from DMF to give compound **3** as yellow crystals, mp 274–275 °C, yield 0.67 g (54%). IR (KBr, cm^{-1}): 2965, 2919 (CH_{aliph}), 1651 ($2C{=}O_{\gamma\text{-pyrone}}$), 1630 ($C{=}O_{quinolinone}$), 1599 (C═N and C═C). ^1H NMR (DMSO-d_6, δ): 1.24 (t, 3H, CH_3, J = 6.6 Hz), 4.43 (q, 2H, J = 6.6 Hz, CH_2), 6.76 (t, 1H, J = 7.2 Hz, Ar—H), 6.93 (d, 1H, J = 6.9 Hz, Ar—H), 7.10 (t, 1H, J = 7.8 Hz, Ar—H), 7.36–7.42 (m, 2H, Ar—H), 7.49 (d, 1H, J = 7.8 Hz, Ar—H), 7.70 (t, 1H, J = 7.2 Hz, Ar—H), 7.99 (d, 1H, J = 7.8 Hz, Ar—H), 8.76 (s, 1H, $H\text{-}4_{pyridine}$). Mass spectrum (m/z, I%): 410 (6), 390 (18), 342 (88), 314 (100), 297 (51), 286 (32), 241 (8), 229 (10), 214 (9), 201 (8), 188 (11), 171 (10), 143 (16), 129 (18), 77 (19). Anal. Calcd for $C_{24}H_{14}N_2O_5$ (410.39): C, 70.24; H, 3.44; N, 6.83%. Found: C, 70.20; H, 3.25; N, 6.49%.

2.2. Characterization methods

Melting point of **ECPPQT** was determined on a digital Stuart SMP3 apparatus. Infrared spectra were measured on Perkin–Elmer 293 spectrophotometer (cm^{-1}), using KBr disks. ^1H NMR spectra were measured on Mercury-300BB (300 MHz), using DMSO-d_6 as a solvent and TMS (δ) as the internal standard. Mass spectra were obtained using GC-2010 Shimadzu Gas chromatography instrument mass spectrometer (70 eV). Elemental microanalyses were performed on a Perkin–Elmer CHN-2400 analyzer. 2-Aminochromone-3-carboxaldehyde (**1**) and 6-ethyl-4-hydroxy-2*H*-pyrano[3,2-*c*]quinoline-2,5(6*H*)-dione (**2**) were prepared according to the literatures (Peterson and Heitzer, 1976 and Kappe et al., 1994).

Morphological characteristics of **ECPPQT** samples were studied by using scanning electron microscopy (SEM) of type JEOL-JSM-636A OLA. The crystalline characteristics of **ECPPQT** samples were investigated by using A Shimadzu X-ray Diffractometer (Model 7000) with utilized monochromatic Cu K_α radiation operated at 30 kV and 30 mA. The diffraction patterns were recorded automatically in the scanning range 2θ = 5°–90° and scan speed 2°/min.

Photoluminescence characteristics of **ECPPQT** were measured using Cary Eclipse Fluorescence Spectrometer, in the wavelength scan range 400–750 nm with scan speed of 500 nm min^{-1}.

Thermal analysis of **ECPPQT** was carried out by differential scanning calorimeter (DSC) using Shimadzu DSC-50.

Optical absorption was measured for films deposited on optically flat corning glass substrate using UV–Vis double beam PC scanning spectrophotometer labomed model UVD-2950 of spectral range 300–1100 nm with a step scan of 2 nm.

Single crystalline wafers of p-type Si were obtained from Nippon Mining Co with area of ~1 cm^2 each and 450 μm thick. The pieces were firstly cleaned and etched by using the CP4 solution ($HF:HNO_3:CH_3COOH$ with ratio 1:6:1). Films of **ECPPQT** were deposited by spin coating on the crystalline substrates to obtain **ECPPQT**/p-Si diode. Ohmic contact was made by high vacuum evaporation of high purity of platinum onto the top of the film and onto the bottom of the substrate using a sputtering unit.

Current–voltage characteristics of **ECPPQT** films were measured by means of high impedance electrometer type Keithley 2635 A attached with a personal computer interfaced via home-made software for recording and plotting for the extracted data from the electrometer. Photoelectrical characteristics were achieved by using a white halogen-tungsten with intensity measured using a solar power meter type TM-206.

3. Results and discussion

3.1. Synthesis characterization

In the present work, the reaction of 2-aminochromone-3-carboxaldehyde (**1**) was studied toward 6-ethyl-4-hydroxy-

2*H*-pyrano[3,2-*c*]quinoline-2,5(6*H*)-dione (**2**) as a heterocyclic enol. Thus, condensation of aldehyde **1** with 6-ethyl-4-hydroxy-2*H*-pyrano[3,2-*c*]quinoline-2,5(6*H*)-dione (**2**) in boiling DMF containing few drops of DBU afforded the heteroannulated chromone 5-ethyl-7*H*,9*H*-chromeno[3″,2″:5′,6′] pyrido[3′,2′:5,6]pyrano[3,2-*c*]quinoline-6(5*H*),7,9-trione (**3**). The reaction may proceed *via* the formation of the condensed intermediate **A** (non-isolable) followed by nucleophilic attack of the amino group at α-lactone carbon (route a) with concomitant α-pyrone ring opening giving intermediate **B** (non-isolable) which underwent an intra molecular cyclodehydration producing the final product **3** as depicted in Fig. 1. Another expected product **4** obtained from cyclo condensation of amino group, in intermediate **A**, with the ketonic carbonyl group (route b) was ruled out based on the spectral data. The IR spectrum of the product revealed the absence of the absorption band assigned to the α-lacone function group, confirming the absence of compound **4**. Moreover, the IR spectrum of compound **3** (Fig. 2) showed absorption bands assigned to $2C{=}O_{\gamma\text{-pyrone}}$ and $C{=}O_{quinolinone}$ at 1651 and 1630 cm^{-1}, respectively. The ^1H NMR spectrum of compound **3** (Fig. 3) showed eight aromatic protons, triplet and quartet signals attributed to the ethyl protons, in addition to a characteristic singlet at δ 8.76 assigned to $H\text{-}4_{pyridine}$. Furthermore, the mass spectrum, shown in Fig. 4, revealed the molecular ion peak at *m*/*z* 410 which is consistent with the expected molecular formula ($C_{24}H_{14}N_2O_5$).

3.2. Thermal analysis characterization

Thermal characteristics are carried out by differential scanning calorimeter (DSC) and the thermogram of this investigation is presented in Fig. 5. As observed, the **ECPPQT** structure is stable up to 530 K. Moreover, a sharp endothermic peak at 546 K was observed, which corresponds to the crystalline melting temperature point of the material.

3.3. Morphology and crystalline structure characterization

The surface morphology of the **ECPPQT** using scanning electron microscope (SEM) with different magnifications is shown in Fig. 6a–d. A rod-like morphology with various lengths and shapes is observed. Moreover, randomly distributed nanorods were obtained and their length ranges from 10 μm to 20 μm and diameter from 100 nm to 400 nm. Pérez-Juste et al. (2005) stated that a nanorods structure is characterized by high sensitivity and can be used for biological sensing applications due to the absorbance band changes with the refractive index of local material. Another trend of applications was suggested by Ayala-Sistos et al. (2005) for gas sensors, video displays, computer components, nano-electronic and nano-optoelectronic components, MEMS devices, and solar energy conversion. Garcia and Semancik (2007) considered the size and shape that affects the basic properties as one of the main factors in their

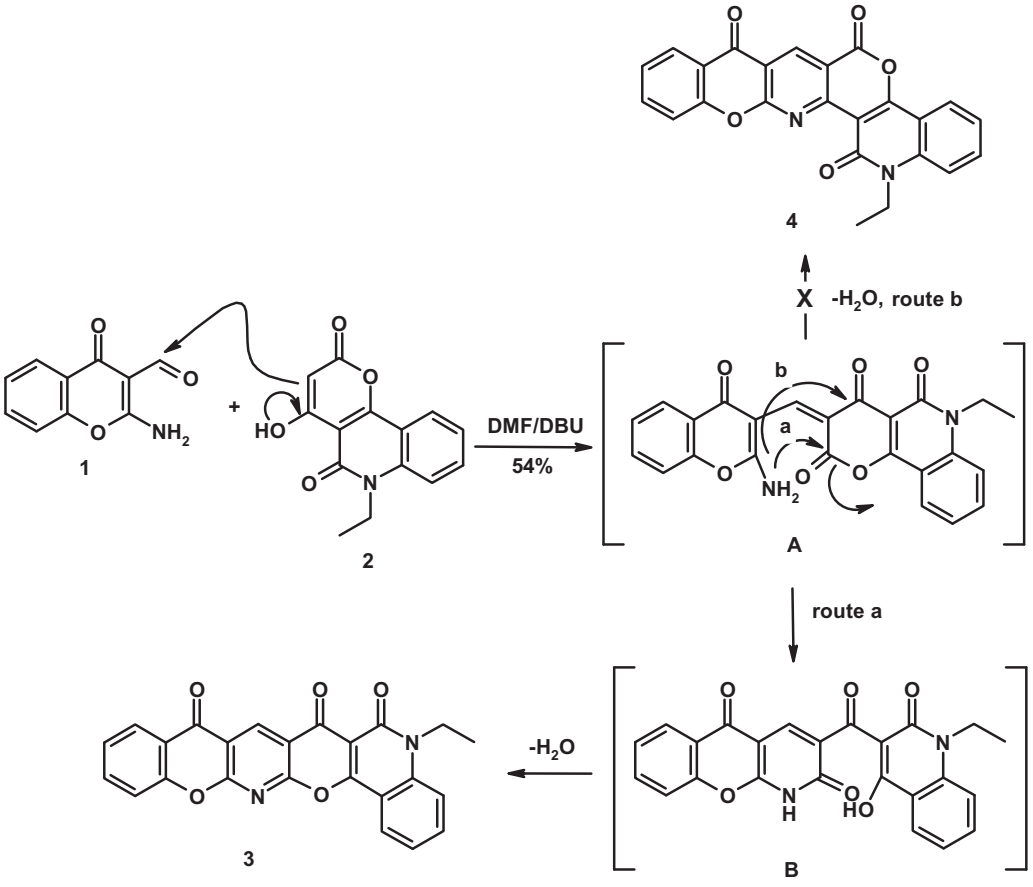

Figure 1 Scheme of the formation of heteroannulated chromone **3**.

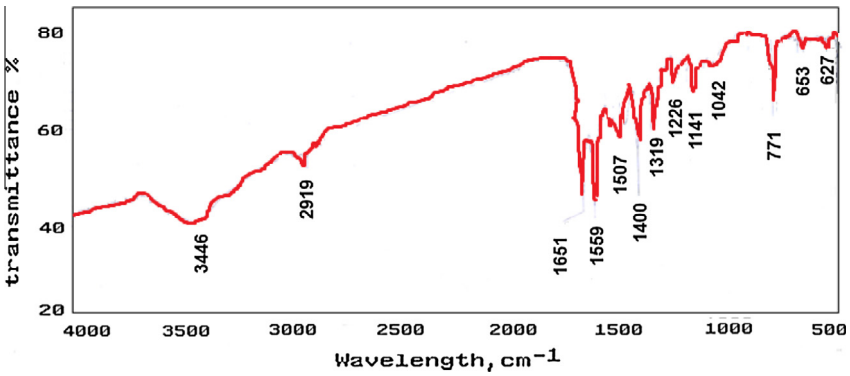

Figure 2 The IR spectrum of **ECPPQT**.

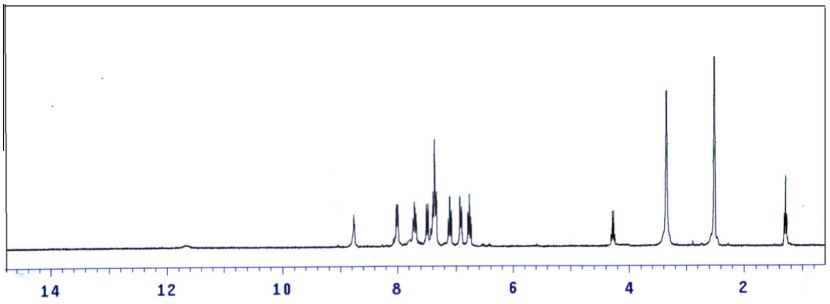

Figure 3 The ^{1}H NMR spectrum of **ECPPQT**.

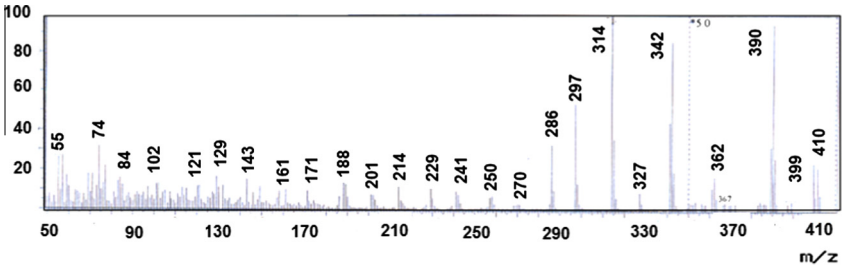

Figure 4 The mass spectrum of **ECPPQT**.

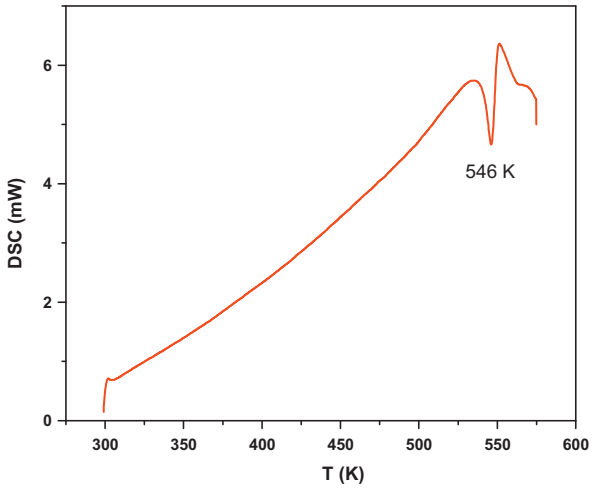

Figure 5 DSC curve of **ECPPQT**.

investigation. Park et al. (2004), Chen et al. (2007) investigated the capability for the structure in nano-electronic and biomedical applications.

The XRD patterns of ECPPQT for the first time are shown in Fig. 7a and b. As observed, a high crystalline feature of the structure with different preferred orientations indicates a polycrystalline structure. The well-known CRYSFIRE computer program (Shirely, 2002) was used for indexing and the inter-planar spacing is compared to the calculated values using "CHECKCELL" program to give an accurate determination for the cell parameters. The crystal investigation confirms that ECPPQT has monoclinic structure with lattice constants of $a = 8.97$ Å, $b = 18.81$ Å, $c = 12.381$ Å and $\beta = 92.05°$. XRD pattern of ECPPQT film, shown in Fig. 2b, performs that the film has also polycrystalline nature with only four significant preferred orientations of (011), (110), (111) and (031) with high background amorphous hump.

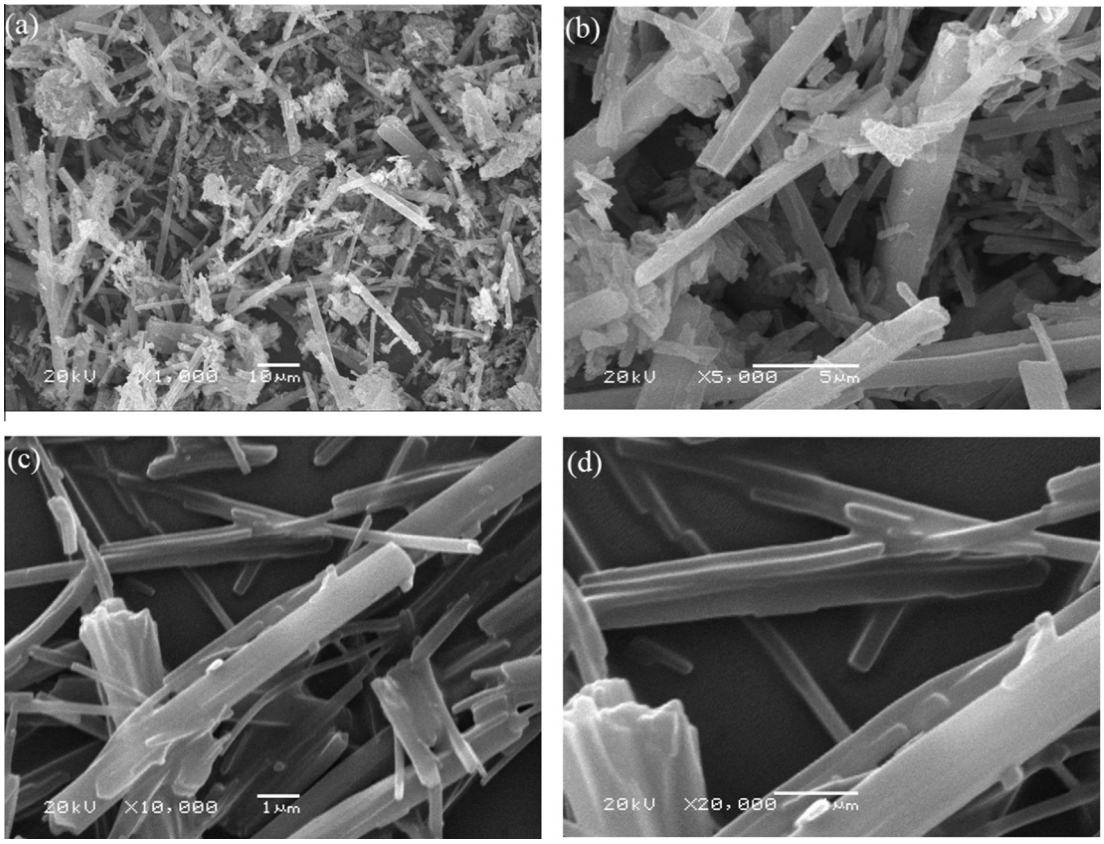

Figure 6 SEM images of **ECPPQT** at different magnifications.

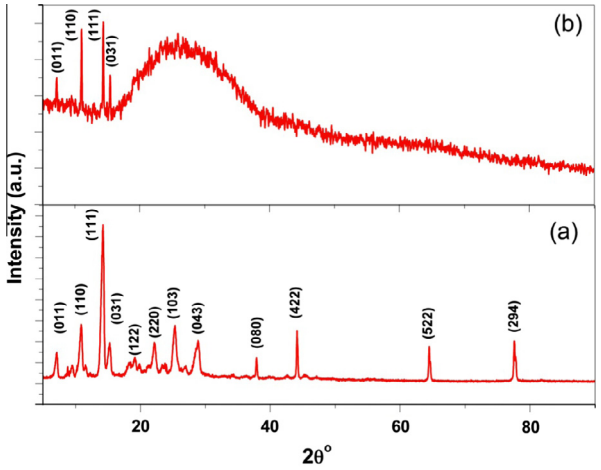

Figure 7 XRD of **ECPPQT** at different magnifications (a) powder and (b) thin film.

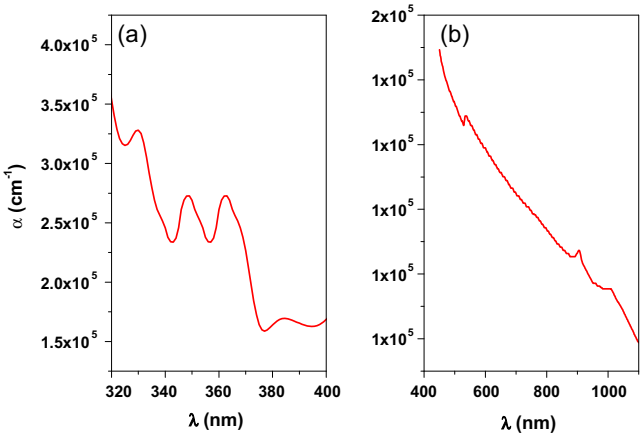

Figure 8 Plot of absorption coefficient vs. λ for **ECPPQT** thin film.

3.4. Optical characterization

The optical absorption characteristics of **ECPPQT** thin films are investigated in the spectral range 200–1100 nm, from which the absorption coefficient, α can easily be calculated by using the well-known simple relation $\left(\alpha = \frac{\ln(1/T)}{d}\right)$ (Yakuphanoglu and Sekerci Evin, 2006), where d is the film thickness, and T is the transmission.

This absorption spectrum is a power tool to investigate the molecular transitions occurring within a material due to electron excitations in the molecule and obtaining the energy gap of organic and inorganic materials as discussed by Issa et al. (2005). Upon light absorbing the energy of the incident photons, some electrons in the ground state will be excited to a higher one. The absorption coefficient spectrum of absorbance spectrum of **ECPPQT** thin film is shown in Fig. 8. The spectrum shows main four absorption bands in the UV region as well as three absorption bands in the Vis region. The bands

appear around 330, 348 and 360 nm can be attributed to the electronic transitions across π–π^* orbitals of aromatic ring. Moreover, the fourth band located at 385 nm involves π–π^* transition of CO and CN groups. The red shift (to longer wavelength) of the transition may be attributed to the conjugation effect as stated in the literature (Issa et al., 2005). In addition, the weak bands located at the longer wavelength band at 547,907 and 1010 nm can be assigned to an intramolecular charge transfer interaction (Kalsi, 2004).

In the strong absorption region, the films have two approximately absorption edges. At higher wavelengths ($\lambda > 1100$ nm), the absorption of film to light tends to zero and then the films become optically transparent. The UV–vis–NIR optical absorption spectroscopy is a well-known tool for calculating the value of optical band gap of organic and inorganic materials.

In organic compounds, the energy difference between the highest occupied molecular orbital (HOMO) and the lowest unoccupied molecular orbital (LUMO) is termed as optical band gap (E_g). The extracted data from the absorption spectrum are modulated into $(\alpha h\nu)^2$ and plotted as a function of photon energy, hν, to estimate the direct band gap values (E_g) of **ECPPQT** films, shown in Fig. 9. The energy band gap can easily be obtained from the extrapolation of the linear part of $(\alpha h\nu)^2$ to zero as shown in Fig. 8. Obviously, there are two direct energy gaps can be extracted depending on the photon energy. These energy gaps are found to be 1.85 and 3.3 eV. Low value of energy gap is termed as optical band gap and can be attributed to the generation of Frankel-exciton, or to a bound electron–hole pair as stated by Hill et al. (2000). But high value of energy gap is called the transport gap energy and corresponds to the difference between HOMO and LUMO as stated by Nayak and Periasamy (2009). The difference between the two energy values can be due to the binding energy of the molecule which is ~1.45 eV. Obviously, in the literature, the exciton binding energy mainly depends on some important parameters such as dielectric constant, molecular size and charge distribution on the molecule. Therefore, high value of the binding energy of the exciton can be attributed to molecular nature and low dielectric constant, generally lies between 0.5 and 1.7 eV (Nayak and Periasamy, 2009; Mir, 2015).

3.5. Photoluminescence characterization

Photoluminescence (PL) spectrum of the sample measured at room temperature (300 K) is shown in Fig. 10. This spectrum was obtained using an excitation wavelength of 350 nm. From this figure, using the Lorentz fitting procedure applied to the figure, the PL spectrum shows broad peaks centered 466, 511, 552 and 602 nm and strong peak located at 704 nm, respectively. Kumar et al. (2011) and Kumar et al. (2009) have confirmed that the PL emission intensity is highly affected by various parameters such as the conjugation length and variation of the substituents of the molecule. Selman et al. (2014) and Ibrahim et al. (2015) have attributed the main strong emission intensity to the radiative recombination of the self-trapped excitons and/or the radiative transitions inside the sub-states initiated from the molecule surface.

3.6. Capacitance–voltage and current–voltage characterization in dark and under illumination

Fig. 11a and b shows the dark and illuminated C–V and C^{-2}–V characteristics under 100 mW/cm^2 at room temperature (~300 K). Obviously, the C–V plots show light sensitivity where the capacitance of the device is dependent of the light intensity under reverse bias voltage at high frequency (1 MHz). This behavior may be attributed to the presence of interface states as discussed by Yahia et al. (2011). Demirezen et al. (2013) have discussed capacitance under illumination by the generation of electron hole pairs in the depletion region of the diode which can be separated under the effect of strong internal electric field. Accordingly, electrons are quickly swept out as compared to holes which may be trapped by the defects (Kim et al., 2011). Thus, there is an additional capacitance in the diode can be considered under illumination.

Semi-logarithmic plot of the forward and reverse biased I–V characteristics of the **ECPPQT**/p-Si diode in dark and illumination conditions of 100 mW/cm^2 at room temperature (300 K) is shown in Fig. 12. Obviously, the diode exhibits rectifying behavior. Moreover, weak voltage dependence for the reverse-bias current as compared to the forward one, and the

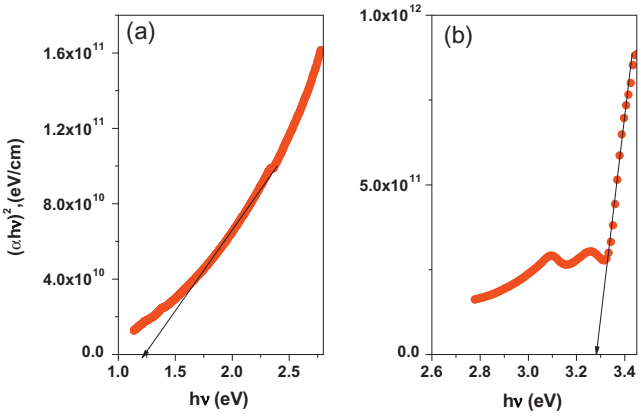

Figure 9 Plot of $(\alpha h\nu)^2$ vs. $h\nu$ (a) first region (b) second region for **ECPPQT** thin film.

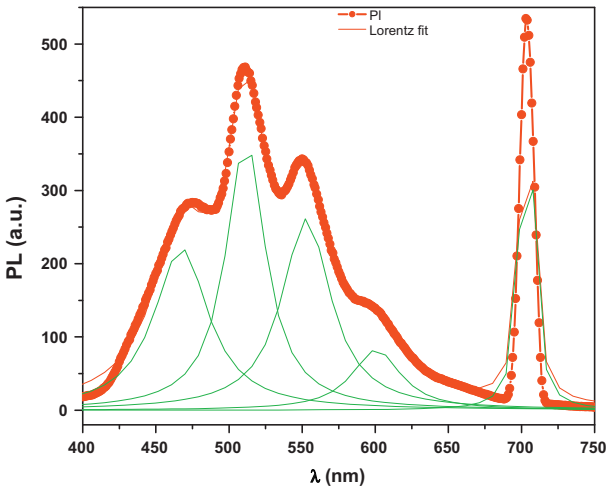

Figure 10 Plot of photoluminescence vs. for **ECPPQT**.

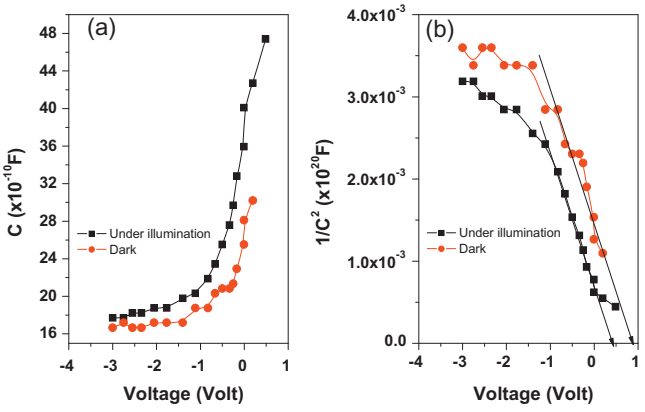

Figure 11 Plot of (a) C vs. V (a) and (b) C^{-2} vs. V in dark and under illumination for **ECPPQT**/p-Si diode.

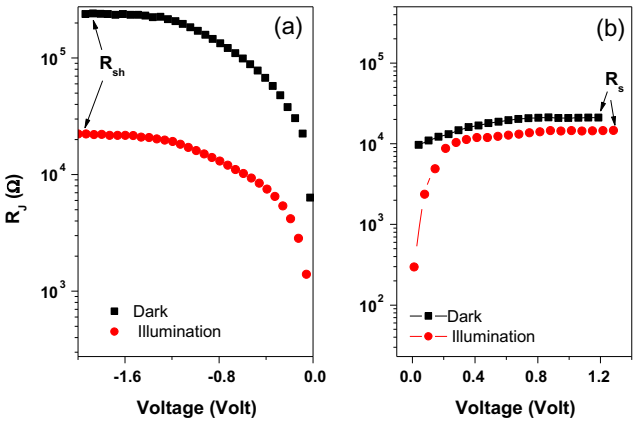

Figure 13 Plot of R_J vs. V in dark and under illumination of 100 mW/cm^2. (a) under reverse bias and (b) under forward bias.

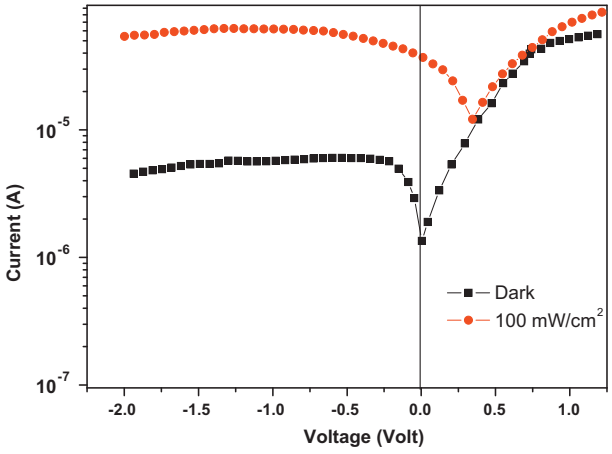

Figure 12 Current–voltage characteristics in dark and under illumination of 100 mW/cm^2.

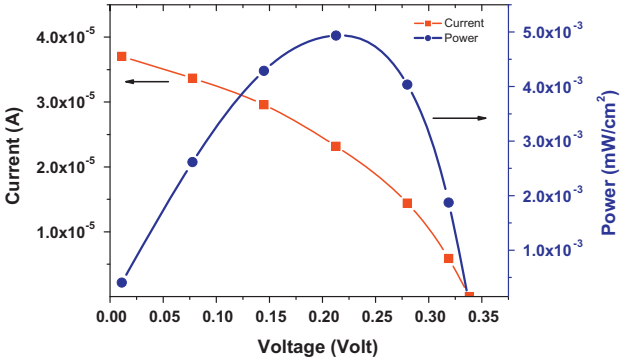

Figure 14 Plot of current vs. V and power vs. V under illumination of 100 mW/cm^2.

exponential increase in the forward-bias current are characteristic properties of rectifying interfaces. In addition, the reverse current of the diodes highly increases with light illumination as compared to the forward one which gives support for the ability for the diode for photodiode applications. Series and shunt resistances for the diode are main factors that affects the diode performance and can easily be determined from the well-known relation ($R_J = \delta V/\delta I$), where R_J is the junction resistance. As observed in Fig. 13, the diode resistance approaches a certain value corresponds to the series resistance, R_s. Moreover, the diode resistance approaches a value correspond to the shunt resistance R_{sh} at sufficiently higher reverse bias. The values of R_s are 2×10^4 and 7×10^3 for the diode in dark and under illumination, respectively. Moreover, the values of R_{sh} are 2×10^5 and 3×10^4 for the diode under dark and illumination, respectively.

When the diode is illuminated, electrons in the valence band of the semiconductor absorb photon energy, and then can jump to the conduction band. Also, the semilogarithmic plot of I–V curves of the diode deviate from linearity at higher forward-bias voltages due to the effects of some important factors such as series resistance and interface states (Aydin et al., 2015). As seen in Fig. 14, the illumination on the reverse I–V characteristics is translated upward moved in the +I direction along the current axis, giving the main photovoltaic parameters such as an open circuit voltage (V_{oc}), short circuit current (I_{sc}), fill factor (FF), and maximum output power (W_{max}) due to the electron–hole pairs generation. Therefore, the reverse current is strongly increased by illumination. The calculated values of V_{oc}, I_{sc}, W_{max} and FF are found to be 3.7×10^{-5} A, 0.33 V, 4.9×10^{-3} mW/cm^2 and 0.40. As observed from the results, the obtained photovoltaic parameters are low as compared with those for the well-known inorganic cells but are acceptable with the other published organic/inorganic photovoltaic cells (Rajesh et al., 2007; El-Nahass et al., 2005, 2007; Yakuphanoglu, 2007a,b).

Moreover, the fabricated diode with **ECPPQT** interfacial layer is more sensitive to light, suggesting them as a good preferred optical sensor or photodiode for optoelectronic applications.

The phototransient current plot of the diode is shown in Fig. 15. As observed, the diode exhibits a good photoconductivity behavior. After switching light on the diode, the photocurrent indicates an abrupt increase in a short time; photocurrent shows almost a stable plateau (reaches stable situation) indicating that the diode has a good stability and quick response properties. The photocurrent of the diode was found to be 0.83 μA. After switching the light off, the photocurrent shows an exponential decrease. The obtained results support

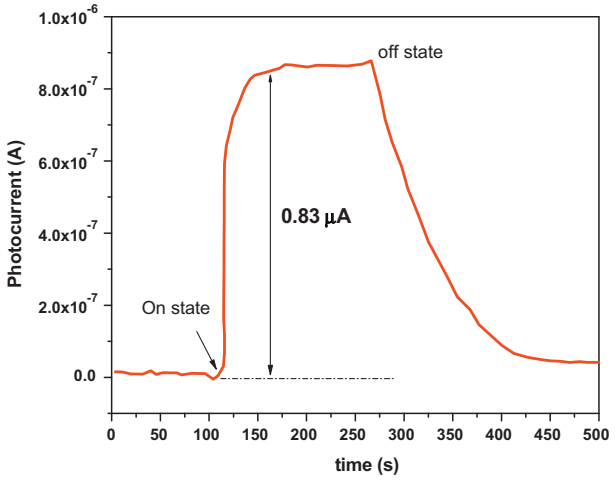

Figure 15 Photocurrent response under influence of light illumination vs. time for **ECPPQT**/p-Si diode.

that the diode can be candidate as a white light photodetector (Yakuphanoglu, 2010).

4. Conclusions

Absorption spectrum of **ECPPQT** films is characterized with various peaks in the UV–Vis–NIR. Moreover, two direct energy gaps were calculated as 3.30 and 1.85 eV. The capacitance of the prepared diodes shows illumination dependent which can be attributed to the improvement of the space charge layer due to the swept of photo-generated charge carriers. Moreover, the decrease in series and shunt resistances under illumination is associated with the generation of charge carriers. The results of photovoltaic characteristic parameters are comparable with those published organic/inorganic photovoltaic diodes. The obtained results suggest that the **ECPPQT** based diode is a promising candidate for optoelectronic applications.

References

Albrecht, U., Lalk, M., Langer, P., 2005. Bioorg. Med. Chem. 13, 1531.
Ashour, A., El Sayed, N.Z., 2009. J. Optoelectron. Adv. Mater. 11, 251.
Ayala-Sistos, J., Rosas, G., Esparza, R., Pérez, B.N.R., 2005. Adv. Technol. Mater. Mater. Proc. 7, 175.
Aydin, H., Tataroğlu, A., Al-Ghamdi, A.A., Yakuphanoglu, F., El-Tantawy, F., Farooq, W.A., 2015. J. Alloys Compds. 625, 18.
Carroll D.L., M., Blau, W., López-Sandoval, R., 2011. J. Nanotechnol., 589241, 2011
Chang, C., Wu Kuo, C.S., Wang, J., Teng, C., 2002. Chin. Pharm. J. 54, 127.
Chavhan, S.D., Senthilarasu, S., Lee, S.H., 2008. Appl. Surf. Sci. 254, 4539.
Chen, T., Zhang, Z., Glotzer, S.C., 2007. Proc. Nat. Acad. Sci. 104, 717.
Cremonesi, A., Bersani, D., Lottici, P.P., Djaoued, Y., Brüning, R., 2006. Thin Solid Films 515, 1500.
Demirezen, S., Altındal, Ş., Uslu, I., 2013. Curr. Appl. Phys. 13, 53.
Deng, Y., Lee, J.P., Ramamonjy, M.T., Synder, J.K., Etages, Des., Kanada, S.A.D., Synder, M.P., Turner, C.J., 2000. J. Nat. Prod. 63, 1082.
Elkington, D., Cooling, N., Belcher, W., Dastoor, P.C., Zhou, X., 2014. Electronics 3, 234.
El-Nahass, M.M., Abd-El-Rahman, K.F., Farag, A.A.M., Darwish, A.A.A., 2005. Org. Electron. 6, 29.
El-Nahass, M.M., Zeyad, H.M., Abd-El-Rahman, K.F., Darwish, A. A.A., 2007. Sol. Energ. Mater. Sol. Cells 91, 1120.
Garcia, S.P., Semancik, S., 2007. Chem. Mater. 19, 4016.
Göker, H., Boykin, D.W., Yıldız, S., 2005. Bioorg. Med. Chem. 13, 1707.
Hill, I.G., Kahn, A., Soos, Z.G., Pascal, R.A., 2000. J. Chem. Phys. Lett. 327, 181.
Hosni, H.M., Abdulla, M.M., 2008. Acta Pharmaceutica 58, 175.
Huang, W., Ding, Y., Miao, Y., Liu, M.Z., Li, Y., Yang, G.F., 2009. Eur. J. Med. Chem. 44, 3687.
Huang, W., Chen, Q., Yang, W.C., Yang, G.F., 2013. Eur. J. Med. Chem. 66, 161.
Ibrahim, M.A.M., 2010. Eur. J. Chem. 1, 124.
Ibrahim, S.S., Allimony, H.A., Abdel-Halim, A.M., Ibrahim, M.A., 2009. Arkivoc xiv, 28.
Ibrahim, M.A., Farag, A.A.M., El-Gohary, N.M., 2015. Synth. Met. 203, 91.
Ishakava, T., Oku, Y., Tanaka, T., Kumamoto, T., 1999. Tetrahedron Lett. 40, 3777.
Issa, R.M., Khedr, A.M., Rizk, H.F., 2005. Spectrochim. Acta Part A 62, 621.
James, D., Scott, S.M., Ali, Z., O'Hare, W.T., 2005. Microchim. Acta 149, 1.
Kalsi, P.S., 2004. Spectroscopy of Organic Compounds, sixth ed. New Age International Publisher, New Delhi.
Kappe, T., Aigner, R., Hohengassner, P., Stadlbauer, W., 1994. J. Prakt. Chem. 336, 596.
Keri, R.S., Budagumpi, S., Pai, R.K., Balakrishna, R.G., 2014. Eur. J. Med. Chem. 78, 340.
Kim, K.S., Gupta, R.K., Chung, G.S., Yakuphanoglu, F., 2011. J. Alloys Compds. 509, 10007.
Knipp, D., 2006. Organic Electronics, (Course Number 300442), Introduction to Organic Electronics. Springer, New York.
Kumar, S., Dutta, J., Dutta, P.K., 2009. J. Macromol. Sci. 46, 1095.
Kumar, S., Dutta, P.K., Koh, J., 2011. Int. J. Biol. Macromol. 49, 356.
Larget, R., Lockhart, B., Renard, P., Largeron, M., 2000. Bioorg. Med. Chem. Lett. 10, 835.
Laukaitish, G., Lindroos, S., Tamulevicius, S., Leskela, M., Rackaitis, M., 2000. Appl. Surf. Sci. 161, 396.
Lee, S.K., Chae, S.M., Yi, K.Y., Kim, N.J., Oh, C.H., 2005. Bull. Korean Chem. Soc. 26, 619.
Li, Z., Li, F., Qin, Liu., Li, T., Ge, R., Meng, W., Tong, J., Xiong, S., Zhou, Y., 2015. Org. Electron. 21, 144.
Lim, L.C., Kuo, Y.C., Chou, C.J., 2000. J. Nat. Prod. 63, 627.
Liu, S.W., Divayana, Y., Sun, X.W., Wang, Y., Leck, K.S., Demir, H. V., 2011. Opt. Express 19, 4513.
Mazzei, M., Sottofattori, E., Dondero, R., Ibrahim, M., Melloni, E., Michetti, M., 1999. Farmaco 53, 452.
Mir, F.A., 2015. Optik 126, 24.
Nayak, P.K., Periasamy, N., 2009. Org. Electron. 10, 1396–1400.
Newman, C.R., Frisbie, C.D., da Silva Filho, D.A., Brédas, J.L., Ewbank, P.C., 2004. Chem. Mater. 16, 4436.
Nohara, A., Ishiguro, T., Ukawa, K., Sugihara, H., Maki, Y., Sanno, Y., 1985. J. Med. Chem. 28, 559.
Park, S., Lim, J.H., Chung, S.W., Mirkin, C.A., 2004. Science 303, 348.
Pérez-Juste, J., Pastoriza-Santos, I., Liz-Marzàn, L.M., Mulvaney, P., 2005. Coord. Chem. Rev. 249, 1870.
Peterson, U., Heitzer, H., 1976. Liebigs Ann. Chem. 23, 1659.
Peumans, P., Yakimov, A., Forrest, S.R., 2003. J. Appl. Phys. 93, 3693.
Pietta, P.J., 2000. J. Nat. Prod. 63, 1035.
Podos, S.D., Thanassi, J.A., Pucci, M.J., 2012. Antimicrob. Agents Chemother. 56, 4095.

Please cite this article in press as: Farag, A.A.M. et al., Synthesis and photoelectrical characterizations of ECPPQT for optoelectronic application. Arabian Journal of Chemistry (2016), http://dx.doi.org/10.1016/j.arabjc.2016.01.002

Rajesh, K.R., Varghese, S., Menon, C.S., 2007. Phys. Chem. Sol. 68, 556.
Sahu, N., Parija, B., Panigrahi, S., 2009. Indian J. Phys. 83, 493.
Selman, A.M., Hassan, Z., Husham, M., Ahmed, N.M., 2014. Appl. Surf. Sci. 305, 445.
Shi, Y.Q., Fukai, T., Sakagami, H., Chang, W.J., Yang, P.Q., Wang, F.P., Nomura, T., 2001. J. Nat. Prod. 64, 181.
Shirely, R., 2002. The CRYSFIRE System for Automatic Powder Indexing: User's Manual The Lattice Press, Guildford, Surrey GU2 7NL, England.
Siddiqui, Z.N., 2012. Tetrahedron Lett. 53, 4974.
Siddiqui, Z.N., Praveen, S., Farooq, F., 2010. Chem. Pap. 64, 818.
Singh, G., Singh, R., Girdhar, N.K., Ishar, M.P.S., 2002. Tetrahedron 58, 2471.
Ukawa, K., Ishiguro, T., Kurik, H., Nohara, A., 1985. Chem. Pharm. Bull. 33, 4432.
Ungwitayatorn, J., Samee, W., Pimthon, J., 2004. J. Mol. Struct. 689, 99–106.
Valenti, P., Bisi, A., Rampa, A., Belluti, F., Gobbi, S., Zampiron, A., Carrara, M., 2000. Bioorg. Med. Chem. 8, 239.
Yahia, I.S., Yakuphanoglu, F., Azim, O.A., 2011. Sol. Energy Mater. Sol. Cells 95, 2598.
Yakuphanoglu, F., 2007a. Synth. Met. 157, 859.
Yakuphanoglu, F., 2007b. Physica B 400, 208.
Yakuphanoglu, F., 2010. J. Alloys Compds. 494, 451.
Yakuphanoglu, F., Arslan, M., 2007. Physica B 393, 304.
Yakuphanoglu, F., Sekerci Evin, M.E., 2006. Physica B 382, 21.
Zhou, Y.H., Fuentes-Hernandez, C., Shim, J., Meyer, J., Giordano, A. J., Li, H., Winget, P., Papadopoulos, T., Cheun, H., Kim, J., Fenoll, M., Dindar, A., Haske, W., Najafabadi, E., Khan, T.M., Sojoudi, H., Barlow, S., Graham, S., Bredas, J.L., Marder, S.R., Kahn Kippelen, A.B., 2012. Science 336, 327.

Please cite this article in press as: Farag, A.A.M. et al., Synthesis and photoelectrical characterizations of ECPPQT for optoelectronic application. Arabian Journal of Chemistry (2016), http://dx.doi.org/10.1016/j.arabjc.2016.01.002